

Fourier time spectral method for subsonic and transonic flows

Lei Zhan^{1,2} · Feng Liu² · Dimitri Papamoschou²

Received: 14 September 2015 / Revised: 30 October 2015 / Accepted: 2 November 2015

© The Chinese Society of Theoretical and Applied Mechanics; Institute of Mechanics, Chinese Academy of Sciences and Springer-Verlag Berlin Heidelberg 2016

Abstract The time accuracy of the exponentially accurate Fourier time spectral method (TSM) is examined and compared with a conventional 2nd-order backward difference formula (BDF) method for periodic unsteady flows. In particular, detailed error analysis based on numerical computations is performed on the accuracy of resolving the local pressure coefficient and global integrated force coefficients for smooth subsonic and non-smooth transonic flows with moving shock waves on a pitching airfoil. For smooth subsonic flows, the Fourier TSM method offers a significant accuracy advantage over the BDF method for the prediction of both the local pressure coefficient and integrated force coefficients. For transonic flows where the motion of the discontinuous shock wave contributes significant higher-order harmonic contents to the local pressure fluctuations, a sufficient number of modes must be included before the Fourier TSM provides an advantage over the BDF method. The Fourier TSM, however, still offers better accuracy than the BDF method for integrated force coefficients even for transonic flows. A problem of non-symmetric solutions for symmetric periodic flows due to the use of odd numbers of intervals is uncovered and analyzed. A frequency-searching method is proposed for problems where the frequency is not known a priori. The method is tested on the vortex shedding problem of the flow over a circular cylinder.

Keywords Fourier time spectral method (TSM) · Pitching airfoil · Transonic flow · Non-symmetric solution · Computational efficiency · Vortex shedding flow · Frequency search

1 Introduction

Time dependent calculations are needed for various important applications, such as the study of the internal flow of turbomachinery, flutter, and jet noise [1–5]. Time accuracy is also needed for large eddy simulation of turbulence-generated noise [6,7] and particle-turbulence interactions [8,9]. In addition to improvements in computer hardware, improvements in numerical methods also play a significant role in reducing the computational cost of time dependent calculations. A dual-time stepping method that was originally developed by Jameson [10] has been successful for unsteady flow computations using both the Euler and the Navier–Stokes equations [11]. Although local pseudo-time stepping, residual smoothing, and multigrid method can be used to accelerate convergence, the computational efficiency of this method is limited. The backward difference formula (BDF) method for the time discretization only provides time accuracy of algebraic orders, specifically 2nd-order for the usual fully implicit three-level BDF scheme. Thus, small real time steps are needed due to the time accuracy requirement.

For periodic flows, an alternative method for real time discretization is to represent flow variables with Fourier series. One of the earliest methods in this category is a linearized method proposed by Hall and Crawley [12]. In this method each flow variable is assumed to be a sum of the time-averaged value and a small perturbation. Based on the small perturbation assumption, the flow governing equation can be simplified and separated into two sets of equations. One is

✉ Feng Liu
fliu@uci.edu

¹ School of Aeronautics, Northwestern Polytechnical University, Xi'an 710072, China

² Department of Mechanical and Aerospace Engineering, University of California, Irvine, CA 92697, USA

for the time-averaged variables, and the other is for the small perturbation components. Coefficients in the latter can be obtained by solving the former. Then the small perturbation components are assumed to be harmonic functions with the known frequency.

To develop an efficient method that can account for nonlinear effects, Ning and He [13] proposed a nonlinear harmonic method. In this method, each flow variable is still expressed as a sum of the time-averaged value and a harmonic perturbation. However, when the nonlinear flow equations are time-averaged, extra “unsteady stress” terms are generated in the time-averaged equations. These extra terms are computed from the solution of the unsteady perturbation equations, while the coefficients of the perturbation equations are determined by the solution of the time-averaged equations. The two sets of equations are solved simultaneously in a strongly coupled manner. Numerical results show that nonlinear effects, such as oscillation of shock waves, can be efficiently modeled by the nonlinear harmonic method.

The nonlinear harmonic method was among the earliest methods that account for a nonlinear effect by reserving extra “unsteady stress” terms in the time-averaged equations. However, the unsteadiness is still evaluated by the first harmonic mode only. Harmonic modes with higher frequencies are not involved. Therefore, the effectiveness of this method is limited for large and complex temporal variations. In addition, the formulation of the method requires a lot of effort, especially for three-dimensional viscous unsteady flow problems. To develop a method that includes more harmonic modes and can be easily applied in engineering practice, Hall et al. [14] proposed the harmonic balance method based on expanding flow variables with Fourier series. In this method the real time derivative term is approximated by the time spectral operator. Fast Fourier transform (FFT) and its inverse counterpart are used in the time spectral operator. The resulting equations on all instants are solved simultaneously in time domain and they are coupled only through the time spectral operator. Since the approximated real time derivative term reduces to a source term, pseudo-time marching method for steady-state calculation can be employed. Convergence accelerating techniques, such as local time step and the multigrid method, can be applied during the pseudo-time marching process without affecting time accuracy. The harmonic balance method has been successfully applied in solving two-dimensional viscous flow past cascades. Computational results show that the method is efficient. Strong nonlinear effects, such as oscillation of shock waves can be accurately predicted if the time resolution is sufficiently high. Gopinath et al. [15] applied the harmonic balance method to the computation of a three-dimensional unsteady flow inside multi-stage turbomachinery. In this computation only one blade passage is used for each blade row. The use of the harmonic balance method greatly reduced the overall cost of the simulation. The dom-

inant unsteadiness and the main flow features, such as the interaction between two blade rows, are captured efficiently. In their study, Ekici et al. [16] completed the computations of three-dimensional periodic inviscid flows around a helicopter rotor using the harmonic balance method. The method was reported to be able to resolve significant unsteady flow features with low computational cost. Since the equations resulting from the harmonic balance method are well-suited for adjoint sensitivity analysis, rotor optimization including improvement of aerodynamic performance and noise reduction can be conveniently conducted.

There were also other ways to calculate periodic flows based on the Fourier expansion of flow variables. A nonlinear frequency domain solver was proposed by McMullen et al. [17], which is equivalent to the harmonic balance method. With this solver the governing equations are solved in the frequency domain rather than the time domain. However, the residual is still calculated in the time domain for simplicity. Transformations between the time domain and the frequency domain for both solutions and residuals are required. This method has been shown to be efficient in solving transonic flows past a pitching airfoil and the vortex shedding flow behind a circular cylinder at rest. A paper by Gopinath and Jameson [18] derived the explicit formula of the approximated real time derivative using the idea of harmonic balance method. Since discrete Fourier transformation and its inverse counterpart are not required in computation, the resulting equations are solved completely in the time domain. For this reason, this variant of the harmonic balance method is called the time spectral method (TSM). We call this method the Fourier TSM since it is based on the Fourier expansion of flow variables. The same work by Gopinath and Jameson [18] also pointed out that stability problem may be caused by the use of even numbers of intervals in a period. Thus, using odd numbers of intervals seems to be favorable. However, we found that non-symmetric solutions are produced for symmetric problems if a period is split into odd numbers of intervals. This problem has not been reported before. We analyze the reason for this problem, and based on that, we propose the requirements to ensure symmetric solutions.

The study by McMullen and Jameson [19] estimated the computational efficiency of the nonlinear frequency domain solver, which is equivalent to the Fourier TSM. The nonlinear frequency domain method is demonstrated to be much more efficient than the 2nd-order BDF method. However, the evaluation is limited to analyzing the error of the computed integration quantities of the surface pressure coefficient, such as the lift coefficient and the moment coefficient. To more comprehensively evaluate the efficiency advantage of the Fourier TSM over the 2nd-order BDF method, we here conduct a systematic error analysis on the computed temporal variation of the surface pressure coefficient itself.

For the periodic flows where the frequency is not known a priori, such as vortex shedding flows, a gradient-based method has been used successfully to search for the frequency [17, 18]. However, the initial guess of the frequency must be close to the correct value since the method is locally optimal. A new method that updates the frequency based on Fourier analysis of the lift coefficient before using the gradient-based method is developed. So the initial guesses of the frequency that are far away from the correct value can be used.

In the following sections, firstly, the Fourier TSM is derived and validated with a transonic flow over the pitching NACA0012 airfoil. For symmetric flow problems, the non-symmetric solutions produced by the use of odd numbers of intervals are discussed. Then error analysis on the surface pressure coefficient and its integration quantities using both the Fourier TSM and the 2nd-order BDF is conducted for transonic flows as well as subsonic flows. Finally, the new frequency search approach is proposed and applied in conjunction with the Fourier TSM to a vortex shedding flow behind a circular cylinder at rest.

2 The Fourier time spectral method (TSM)

The Navier–Stokes equations for a two-dimensional compressible viscous flow can be written as

$$\frac{\partial \mathbf{w}}{\partial t} + \frac{\partial \mathbf{f}_c}{\partial x} + \frac{\partial \mathbf{g}_c}{\partial y} - \frac{\partial \mathbf{f}_v}{\partial x} - \frac{\partial \mathbf{g}_v}{\partial y} = \mathbf{0}, \tag{1}$$

where

$$\mathbf{w} = \begin{pmatrix} \rho \\ \rho u \\ \rho v \\ \rho E \end{pmatrix}, \mathbf{f}_c = \begin{pmatrix} \rho \bar{u} \\ \rho u \bar{u} + p \\ \rho v \bar{u} \\ \rho E \bar{u} + p u \end{pmatrix}, \mathbf{g}_c = \begin{pmatrix} \rho \bar{v} \\ \rho u \bar{v} \\ \rho v \bar{v} + p \\ \rho E \bar{v} + p v \end{pmatrix}, \tag{2}$$

$$\mathbf{f}_v = \begin{pmatrix} 0 \\ \tau_{xx} \\ \tau_{yx} \\ u \tau_{xx} + v \tau_{yx} - q_x \end{pmatrix}, \mathbf{g}_v = \begin{pmatrix} 0 \\ \tau_{xy} \\ \tau_{yy} \\ u \tau_{xy} + v \tau_{yy} - q_y \end{pmatrix}. \tag{3}$$

In the preceding equations, t is time, x and y are position coordinates, ρ is density, p is pressure, (u, v) is the local flow velocity. The total energy is $E = e + \frac{1}{2}(u^2 + v^2)$ with internal energy $e = \frac{p}{(\gamma-1)\rho}$. γ is the ratio of specific heat. $(\bar{u}, \bar{v}) = (u - u_b, v - v_b)$ stands for the local convective velocity relative to the control surface moving at the velocity of (u_b, v_b) . The components of the viscous stress tensor and those of the heat flux vector are defined as below

$$\begin{aligned} \tau_{xx} &= 2\mu \left[\frac{\partial u}{\partial x} - \frac{1}{3} \left(\frac{\partial u}{\partial x} + \frac{\partial v}{\partial y} \right) \right], \\ \tau_{yx} &= \tau_{xy} = \mu \left(\frac{\partial u}{\partial y} + \frac{\partial v}{\partial x} \right), \\ \tau_{yy} &= 2\mu \left[\frac{\partial v}{\partial y} - \frac{1}{3} \left(\frac{\partial u}{\partial x} + \frac{\partial v}{\partial y} \right) \right], \\ q_x &= -\frac{\mu}{Pr} \frac{\partial h}{\partial x}, \\ q_y &= -\frac{\mu}{Pr} \frac{\partial h}{\partial y}, \end{aligned} \tag{4}$$

where μ is the molecular viscosity, which is calculated by Sutherland’s law. Pr is the Prandtl number, $h = e + \frac{p}{\rho}$ is enthalpy.

If the unsteady flow is periodic, then the flow solution vector \mathbf{w} can be expanded using the Fourier series as below

$$\mathbf{w}(t) = \sum_{-\infty}^{+\infty} \tilde{w}_k e^{ik\omega t}, \tag{5}$$

where ω is the fundamental angular frequency of the periodic flow. The Fourier coefficient \tilde{w}_k can be calculated as

$$\tilde{w}_k = \frac{\omega}{2\pi} \int_0^{\frac{2\pi}{\omega}} \mathbf{w}(t) e^{-ik\omega t} dt, k = 0, \pm 1, \pm 2, \dots \tag{6}$$

If finite harmonic modes are retained in the series of Eq. (5), discrete Fourier transform (DFT) pair can be constructed. Assume a period is equally divided into N intervals, then the solution vectors on the left N instants form the following time sequence, which is the extended solution vector

$$\mathbf{w}^* = [w_0, \dots, w_n, \dots, w_{N-1}]^T. \tag{7}$$

The DFT on the above extended solution vector is written as

$$\tilde{w}_k = \frac{1}{N} \sum_{n=0}^{N-1} w_n e^{-ik\omega n \Delta t}, \tag{8}$$

where $\Delta t = \frac{2\pi}{\omega N}$. If N is odd, the inverse DFT (IDFT) is written as

$$w_n = \sum_{k=-\frac{N-1}{2}}^{\frac{N-1}{2}} \tilde{w}_k e^{ik\omega n \Delta t}. \tag{9}$$

When N is even, the inverse DFT is modified as

$$w_n = \sum_{k=-\frac{N}{2}}^{\frac{N}{2}-1} \tilde{w}_k e^{ik\omega n \Delta t}. \tag{10}$$

In matrix form, the DFT in Eq. (8) can be expressed as

$$\tilde{\mathbf{w}}^* = \mathbf{E} \mathbf{w}^*, \tag{11}$$

where \mathbf{E} is the DFT operator matrix. $\tilde{\mathbf{w}}^*$ is the Fourier coefficient vector of solution. If N is odd,

$$\tilde{\mathbf{w}}^* = [\tilde{w}_0, \tilde{w}_{-1}, \dots, \tilde{w}_{-\frac{N-1}{2}}, \tilde{w}_{\frac{N-1}{2}}, \dots, \tilde{w}_1]^T. \tag{12}$$

When N is even, $\tilde{\mathbf{w}}^*$ becomes

$$\tilde{\mathbf{w}}^* = [\tilde{w}_0, \tilde{w}_{-1}, \dots, \tilde{w}_{-\frac{N}{2}+1}, \tilde{w}_{-\frac{N}{2}}, \tilde{w}_{\frac{N}{2}-1}, \dots, \tilde{w}_1]^T. \tag{13}$$

For the IDFT in Eq. (9) or Eq. (10), it can be expressed in matrix form as

$$\mathbf{w}^* = \mathbf{E}^{-1} \tilde{\mathbf{w}}^*, \tag{14}$$

where \mathbf{E}^{-1} is the IDFT operator matrix. \mathbf{w}^* and $\tilde{\mathbf{w}}^*$ form the DFT pair for flow solution. Since the first-order derivative of a periodic function is also a periodic function, the DFT pair for the time derivative of flow solution can be constructed as well. The corresponding DFT and IDFT are

$$\tilde{\mathbf{w}}^{(1)*} = \mathbf{E} \mathbf{w}^{(1)*} \tag{15}$$

and

$$\mathbf{w}^{(1)*} = \mathbf{E}^{-1} \tilde{\mathbf{w}}^{(1)*}, \tag{16}$$

where the extended vector in time domain $\mathbf{w}^{(1)*} = [\frac{\partial w}{\partial t}|_0, \dots, \frac{\partial w}{\partial t}|_n, \dots, \frac{\partial w}{\partial t}|_{N-1}]^T$, and $\tilde{\mathbf{w}}^{(1)*}$ is the Fourier coefficient vector for the time derivative of flow solution. The k -th element of $\tilde{\mathbf{w}}^{(1)*}$ can be calculated from the k -th element of $\tilde{\mathbf{w}}^*$ through the following relation:

$$\tilde{w}_k^{(1)*} = ik\omega \tilde{w}_k. \tag{17}$$

Written in matrix form, $\tilde{\mathbf{w}}^{(1)*}$ can be formulated as

$$\tilde{\mathbf{w}}^{(1)*} = i\omega N_F \tilde{\mathbf{w}}^*, \tag{18}$$

where N_F is a diagonal matrix. If N is odd, $N_F = \text{diag}(0, -1, \dots, -\frac{N-1}{2}, \frac{N-1}{2}, \dots, 1)$. When N is even, $N_F = \text{diag}(0, -1, \dots, -\frac{N}{2} + 1, 0, \frac{N}{2} - 1, \dots, 1)$.

In TSM, the extended time derivative vector $\mathbf{w}^{(1)*}$ can be calculated from \mathbf{w}^* through DFT and IDFT as below

$$\mathbf{w}^{(1)*} = \mathbf{E}^{-1} \tilde{\mathbf{w}}^{(1)*} = i\omega \mathbf{E}^{-1} N_F \tilde{\mathbf{w}}^* = i\omega \mathbf{E}^{-1} N_F \mathbf{E} \mathbf{w}^* = \mathbf{F} \mathbf{w}^*, \tag{19}$$

where \mathbf{F} denotes the time spectral operator, which is an $N \times N$ matrix. If N is even, the DFT and IDFT can be replaced by FFT and IFFT so as to evaluate the time spectral operator efficiently. The element at the l -th row and the n -th column of the time spectral operator matrix, $F_{l,n}$ ($0 \leq l, n \leq N - 1$), can be expressed as

$$F_{l,n} = \frac{\omega}{N} \sum_{k=-\frac{N}{2}+1}^{\frac{N}{2}-1} ik e^{\frac{2\pi ik}{N}(l-n)} = \begin{cases} \frac{\omega}{2} (-1)^{(l-n)} \cot[\frac{\pi(l-n)}{N}], & l \neq n, \\ 0, & l = n. \end{cases} \tag{20}$$

Note that the fundamental angular frequency of a periodic flow problem ω is an explicitly specified parameter inside the time spectral operator.

Following the method of lines, the unsteady governing equation (1) can be integrated over grid cells using the cell-centered finite volume method. The governing equations in the semi-discrete form on N equally spaced instants can be collected together and written as

$$\frac{d\mathbf{w}^*}{dt} + \mathbf{R}(\mathbf{w}^*) = \mathbf{0}. \tag{21}$$

Using the Fourier TSM to solve the above equation, the time derivative term of the equation can be approximated by the time spectral operator. The resultant equation becomes

$$\mathbf{F} \mathbf{w}^* + \mathbf{R}(\mathbf{w}^*) = \mathbf{0}. \tag{22}$$

The above equation takes the form of governing equation for steady problems. There is no explicit time derivative and the time derivative term reduces to a source term. To solve such a system, pseudo-time marching technique is usually adopted. Introducing the pseudo-time τ , the final equation to be solved is

$$\frac{d\mathbf{w}^*}{d\tau} + \mathbf{F} \mathbf{w}^* + \mathbf{R}(\mathbf{w}^*) = \mathbf{0}. \tag{23}$$

In Eq. (23), $\mathbf{R}(\mathbf{w}^*)$ is calculated by the Jameson-Schmidt-Turkel (JST) scheme [20]. The pseudo-time marching process is conducted by a five-stage explicit Runge–Kutta scheme because of its extended stability range. The fully discretized governing equations on all instants are coupled only through the time spectral operator and are solved simultaneously in time domain as in Ref. [14]. Convergence acceleration technique, such as local time stepping and multigrid method, can be used during pseudo-time marching without losing time accuracy.

3 Application to the pitching airfoil test case

The periodic flows over a pitching NACA0012 airfoil at transonic flow conditions are frequently used as test cases for unsteady solvers. For this reason, the Fourier TSM is validated by solving an inviscid test case of this kind. Computational results using the Fourier TSM is also compared with those using the BDF method. In the present inviscid test case, a NACA0012 airfoil is forced to pitch around its quarter chord at $M_\infty = 0.755$. The forced pitching movement is given by

$$\alpha = \alpha_0 + \alpha_m \sin \omega t, \tag{24}$$

where α_0 is the mean angle of attack, α_m the pitching amplitude. ω is the angular frequency and is related to the reduced frequency κ as

$$\kappa = \frac{\omega c}{2U_\infty}, \tag{25}$$

where c is the chord length and U_∞ is the free-stream velocity. In this case, $\alpha_0 = 0.016^\circ$, $\alpha_m = 2.51^\circ$, and $\kappa = 0.0814$. The periodic inviscid flow in this test case is calculated on a 161×33 O-type grid. The convergence criteria is set to be 1×10^{-14} . To implement the Fourier TSM, three different time resolutions are used. One period is equally split into 8, 16, or 32 intervals, respectively. For the BDF method, 32 or 64 equal intervals are used.

The computed lift and moment coefficient variations with respect to the angle of attack are shown in Fig. 1. The experimental data at Reynold's number $Re = 5.5 \times 10^6$ [21] are also shown to demonstrate the same general agreement between the computations and the experiment as found in Gao et al. [22,23], despite the noticeable differences due to negligence of viscous and turbulence effects by the Euler equations. The purpose of this paper is to investigate the time spectral method vs. the conventional BDF time-marching method in resolving

time evolution for the Euler equations. Therefore, the computational result using the BDF method with 64 time intervals is used as the benchmark accurate solution in the following discussions. Figure 1a shows that for the lift coefficient, the computational result using the Fourier TSM only with eight intervals agrees very well with the accurate solution. For the moment coefficient, Fig. 1b shows that the computational results using the Fourier TSM converge fast to the accurate solution as time resolution increases. However, to predict well all details of the temporal variation of the moment coefficient, at least 16 intervals are needed for the Fourier TSM. Compared to the temporal variation of the lift coefficient, that of the moment coefficient is more complicated. Hence, to reach the same level of accuracy, more intervals (more Fourier modes in the frequency domain) are required for the Fourier TSM to calculate the latter.

As for the temporal variation of the surface pressure coefficient distribution, it is convenient to show it in frequency domain. The time-averaged component and the first three modes are shown in Figs. 2, 3, 4, and 5. Computa-

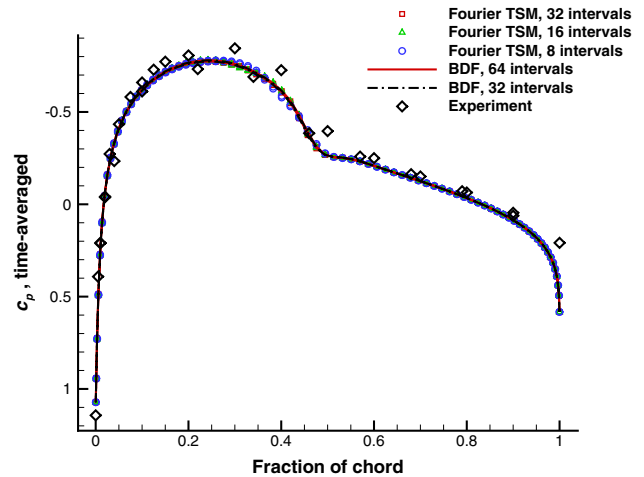


Fig. 2 Inviscid flow over pitching NACA0012 airfoil: time-averaged surface pressure coefficient

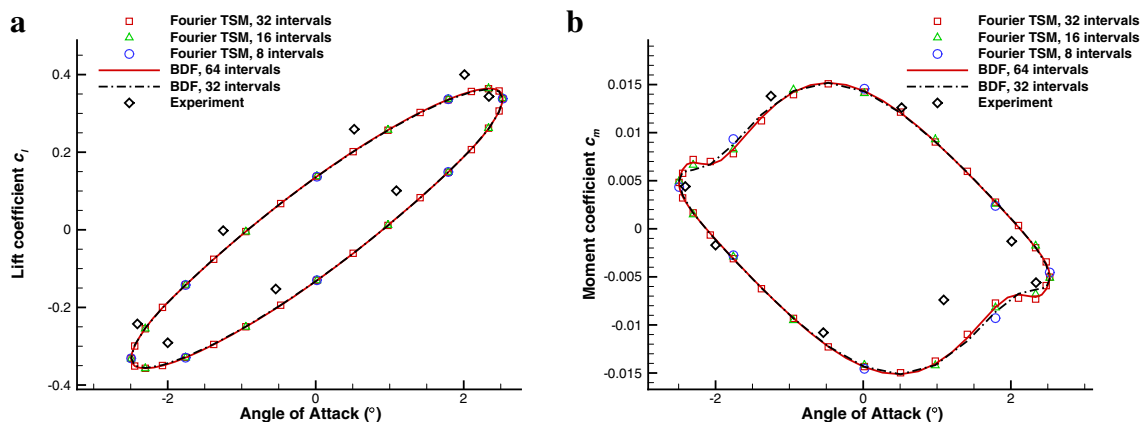


Fig. 1 Inviscid flow over pitching NACA0012 airfoil: lift and moment coefficients versus angle of attack. **a** Lift coefficient. **b** Moment coefficient

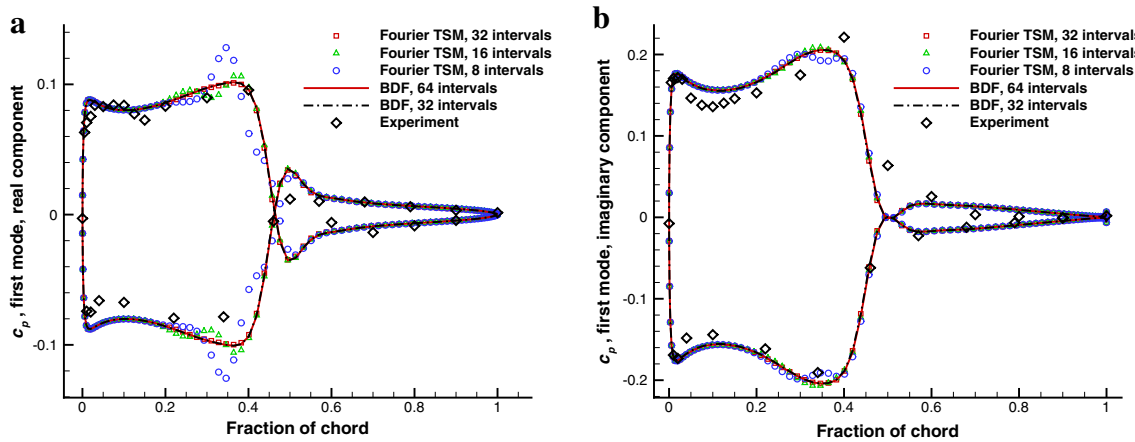


Fig. 3 Inviscid flow over pitching NACA0012 airfoil: first mode of surface pressure coefficient. **a** Real component. **b** Imaginary component

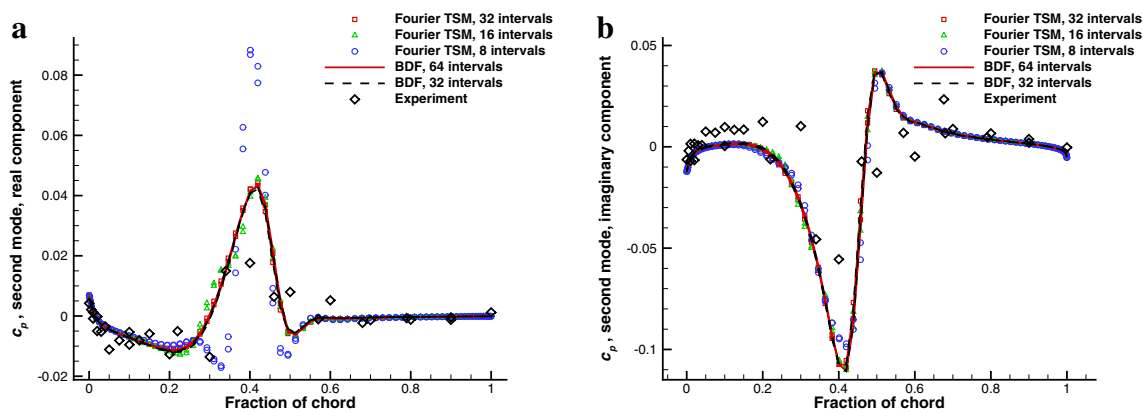


Fig. 4 Inviscid flow over pitching NACA0012 airfoil: second mode of surface pressure coefficient. **a** Real component. **b** Imaginary component

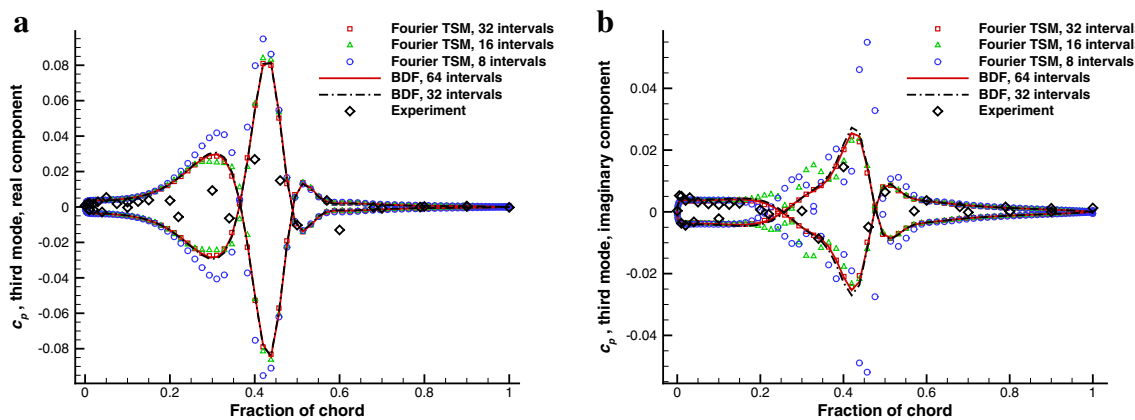


Fig. 5 Inviscid flow over pitching NACA0012 airfoil: third mode of surface pressure coefficient. **a** Real component. **b** Imaginary component

tional results as well as experimental data [21] all reveal that the range of the shock wave movement is approximately $0.2 < x/c < 0.6$. Within this area, the Fourier TSM with eight intervals in a period can only reasonably predict the time-averaged component of the surface pressure coefficient. When time resolution increases to have 16 intervals in a period, the Fourier TSM could also generally

resolve the first mode, the second mode and the real component of the third mode. For the imaginary component of the third mode, Fig. 5b shows that the computational result using the Fourier TSM with 16 intervals deviates dramatically from the accurate solution. To make improvement on this, 32 intervals are needed. Outside the shock wave movement area ($x/c < 0.2$ or $x/c > 0.6$), the Fourier TSM with

only eight intervals could perfectly resolve the time-averaged component and all three modes of the surface pressure coefficient. This is because in the shock-free area, the temporal variation of the surface pressure coefficient is smooth, its Fourier modes with high frequencies decay rapidly. Thus, only retaining the first three modes (corresponding to eight intervals) is sufficient for the Fourier TSM to obtain accurate computational results. Since the temporal variation of the surface pressure coefficient could be perfectly predicted in most area, the Fourier TSM with only eight intervals is able to calculate accurately the integration quantities, in particular the lift coefficient. For the moment coefficient, the accuracy loss of the surface pressure coefficient in the area of shock wave movement only affects some details of its temporal variation. The general trend and the range of the temporal variation are about correct.

4 Non-symmetric solutions of symmetric problems due to odd numbers of intervals

When the Fourier TSM is applied to solve periodic flow problems, proper time resolution should be carefully selected to balance accuracy of the solution and computational cost. Another important issue is whether the number of intervals is even or odd. Gopinath and Jameson [18] pointed out that the use of an even number of intervals may cause stability problem for the Fourier TSM, particularly in the cases where the time derivative is significant, such as high RPM turbomachinery problems. This is because the odd-even decoupled solution may be allowed when the Fourier TSM is applied with an even number of intervals. Thus, using odd numbers of intervals seems to be favorable. However, we found that the Fourier TSM produces non-symmetric solutions for symmetric flow problems if an odd number of intervals are employed. To illustrate this, a symmetric flow problem is constructed from the previous test case and is solved by the Fourier TSM. In this symmetric flow problem, the airfoil still pitches around its quarter chord point. All the flow conditions remain the same except that the mean angle of attack is set to be zero. Under these flow conditions, the periodic flow past the airfoil is symmetric given that the airfoil is symmetric. For this symmetric flow, the distribution of the surface pressure coefficient on the upper surface should be perfectly symmetric to or overlap that on the lower surface in frequency domain. The computed time-averaged component and the first three Fourier modes are shown in Figs. 6, 7, 8, and 9, respectively. For the Fourier TSM, seven or eight intervals are used. The solution obtained by the BDF method with 32 intervals serves as a reference solution. It is observed that when eight intervals are used, the solution from the Fourier TSM is symmetric, just like the reference solution. This is true for any Fourier mode of the pressure coefficient in any surface area. Whereas,

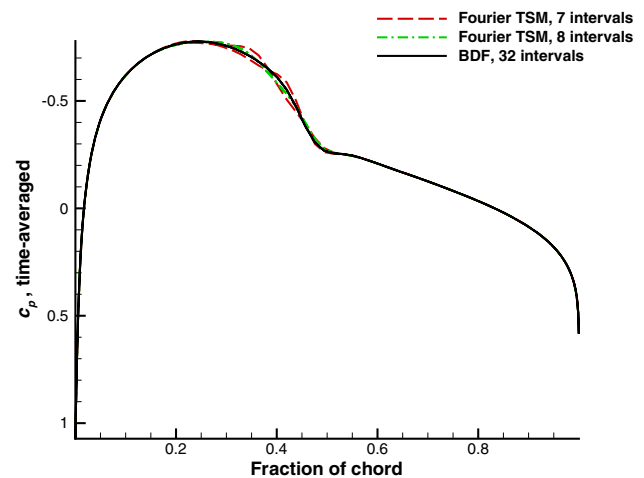


Fig. 6 Symmetric inviscid flow over pitching NACA0012 airfoil: time-averaged surface pressure coefficient

if seven intervals are employed, non-symmetric solution is produced by the Fourier TSM, especially in the area where shock wave moves. Outside the area of shock wave movement, the solution is still non-symmetric and the asymmetry becomes quite weak.

Whether the asymmetry of the solution using seven intervals in a certain area is obvious or not actually depends on if seven intervals are sufficient to resolve the local unsteady flow. The computational results of the previous test case for validation have shown that using eight intervals could only retain three Fourier modes in the Fourier TSM. This is not sufficient to resolve the shock wave movement. Thus, the calculated surface pressure coefficient exhibits dramatic error in the area where shock wave moves. Using seven intervals can only retain the first three Fourier modes in the Fourier TSM as well. Thus, the error of the computed surface pressure coefficient is also high in the same surface area. This is why the asymmetry of the solution using seven intervals is obvious. It can be anticipated that if time resolution is increased so as to retain more Fourier modes in the Fourier TSM, the asymmetry of solutions using odd numbers of intervals will decrease in the area of shock wave movement.

Actually, the problem of non-symmetric solution of a symmetric problem due to the use of odd numbers of intervals is not limited to the Fourier TSM. Numerical experiments have confirmed that the same problem also happens to the BDF method. The reason for this problem is not associated with the specific method of time discretization, but lies in the way independent instants (not including the one at the end of a period) are distributed in a period. To guarantee symmetric solutions for symmetric flow problems, we propose that the distribution of independent instants should satisfy the following requirements. All independent instants should be able to be grouped into pairs, and the phase difference between

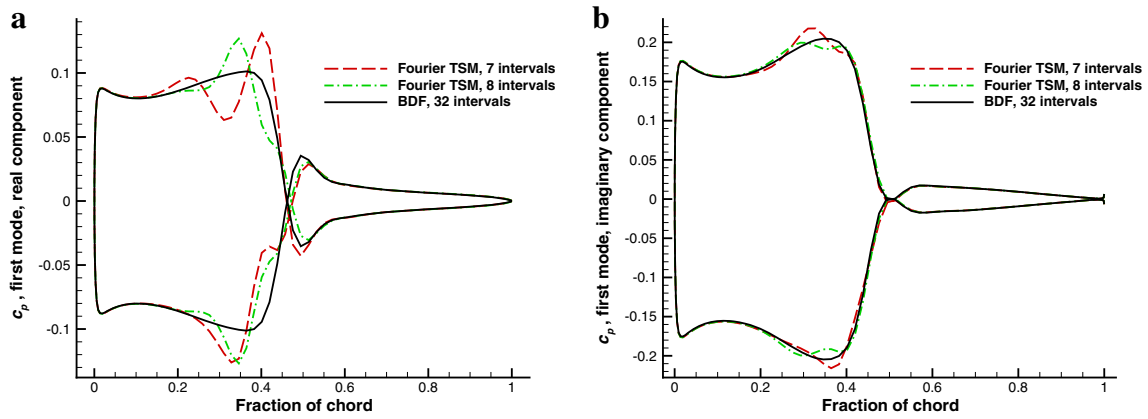


Fig. 7 Symmetric inviscid flow over pitching NACA0012 airfoil: first mode of surface pressure coefficient. **a** Real component. **b** Imaginary component

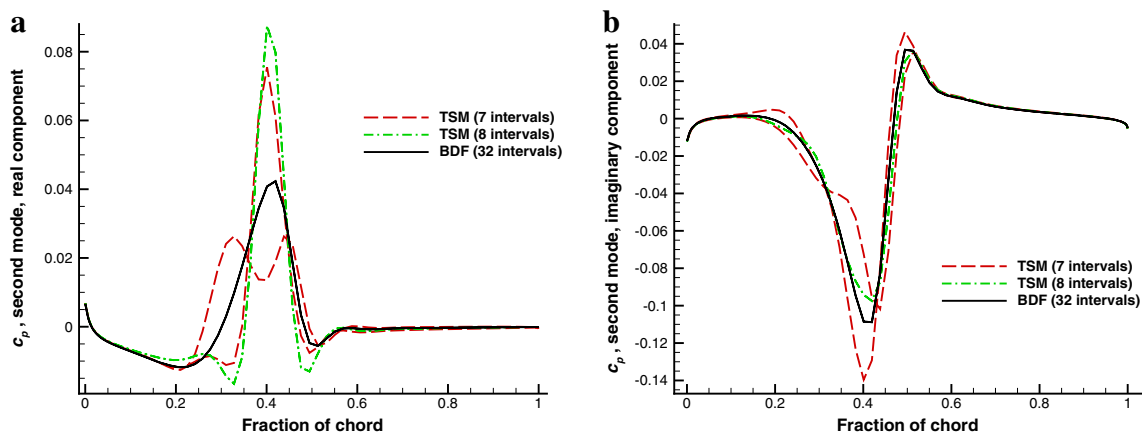


Fig. 8 Symmetric inviscid flow over pitching NACA0012 airfoil: second mode of surface pressure coefficient. **a** Real component. **b** Imaginary component

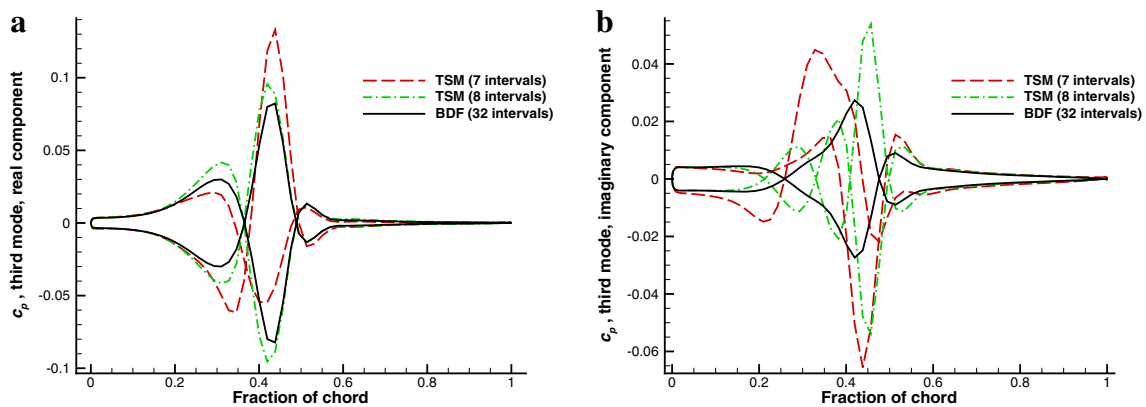


Fig. 9 Symmetric inviscid flow over pitching NACA0012 airfoil: third mode of surface pressure coefficient. **a** Real component. **b** Imaginary component

each pair of independent instants should be 180° . Apparently, splitting a period into eight equal intervals (or other even numbers of intervals) automatically satisfies all these requirements. Hence, the solution for a symmetric problem

is symmetric. If a period is divided into seven equal intervals (or other odd numbers of intervals), it is impossible to group all the independent instants into pairs since the number of independent instants is odd. Thus, the requirements

are not satisfied and the solution for a symmetric problem is non-symmetric.

For the reason discussed above, we choose to use even numbers of equal intervals in a period for the Fourier TSM as long as the computation can converge. Gopinath also justified that the Fourier TSM using an even number of intervals is usually stable for problems where the time derivative is relatively small, such as the flow past pitching airfoils and wings at low forced frequencies [18]. In any of the present computations using the Fourier TSM with even numbers of intervals, the stability problem is not encountered. A possible reason is that the frequencies in these flow problems are not high enough to trigger the stability problem. In addition to using even numbers of intervals, we also make sure that the number of intervals is a power of 2 since efficient FFT can be directly used in the Fourier TSM.

5 Error analysis on solutions for transonic and subsonic flows

For smooth flows, time resolution by the Fourier TSM should be of exponential order of accuracy as compared to the 2nd-order time accuracy of the BDF scheme used in Ref. [11]. However, this may not be the case for flows with shock motion. To evaluate comprehensively the computational efficiency of the Fourier TSM and compare it to that of the BDF method, error analysis is conducted to the computed solutions. The previous test case for validation has shown that whether or not shock wave movement exists has a great influence on the time accuracy of the Fourier TSM. For this reason, two flow problems are solved to provide solutions for error analysis. The first one is still the previous test case for validation, in which the NACA0012 airfoil pitches around its quarter chord point with $M_\infty = 0.755$, $\alpha_0 = 0.016^\circ$, $\alpha_m = 2.51^\circ$, and $\kappa = 0.0814$. In this flow problem, shock waves move back and forth over airfoil surface. For the purpose of convenient comparison, the second flow problem is constructed from the first one. In the constructed flow problem, all the flow conditions remain the same except that the free stream Mach number is lowered to $M_\infty = 0.6$. Computational results show that the flow of this problem is subsonic everywhere. Hence, this flow problem is shock-free. To conduct error analysis, five different time resolutions are used for the Fourier TSM. Corresponding to these time resolutions, a period is split into 4, 8, 16, 32, or 64 equal intervals. When the BDF method is applied, 16, 32, or 64 equal intervals are used in a period. The solution using the Fourier TSM with 64 intervals is selected as the accurate solution. To ensure the reliability of the error analysis, computations using the Fourier TSM and the BDF method all converge to the residual level of 1×10^{-14} .

McMullen and Jameson [19] chose to use lift and moment coefficients as figures-of-merit when evaluating the computational efficiency of the Fourier TSM. As the first step of the present error analysis, we follow the same idea to work on the computed lift and moment coefficients as well. For any computed solution, the squared error of the lift coefficient in a period is defined as follows

$$\begin{aligned} \text{Error}_{c_l}^2 = & \sum_{n=0}^m \left[(\text{Re}_n(c_l) - \text{Re}_n(c_{l,a}))^2 \right. \\ & \left. + (\text{Im}_n(c_l) - \text{Im}_n(c_{l,a}))^2 \right] \\ & + \sum_{n=m+1}^{m_a} \left[(\text{Re}_n(c_{l,a}))^2 + (\text{Im}_n(c_{l,a}))^2 \right], \end{aligned} \quad (26)$$

where $\text{Re}_n(c_l)$ and $\text{Im}_n(c_l)$ are the real and imaginary components of the n -th Fourier mode of the lift coefficient for the given solution. $\text{Re}_n(c_{l,a})$ and $\text{Im}_n(c_{l,a})$ are the real and imaginary components of the n -th Fourier mode of the lift coefficient for the accurate solution. m and m_a are the numbers of Fourier modes that the given solution and the accurate solution include, respectively. The first summation in the Eq. (26) represents the aliasing error of the given solution, whereas the second one is a measure of the truncation error of the same solution. Similarly, for any computed solution, the squared error of the moment coefficient in a period can be defined as follows

$$\begin{aligned} \text{Error}_{c_m}^2 = & \sum_{n=0}^m \left[(\text{Re}_n(c_m) - \text{Re}_n(c_{m,a}))^2 \right. \\ & \left. + (\text{Im}_n(c_m) - \text{Im}_n(c_{m,a}))^2 \right] \\ & + \sum_{n=m+1}^{m_a} \left[(\text{Re}_n(c_{m,a}))^2 + (\text{Im}_n(c_{m,a}))^2 \right], \end{aligned} \quad (27)$$

where $\text{Re}_n(c_m)$ and $\text{Im}_n(c_m)$ are the real and imaginary components of the n -th Fourier mode of the moment coefficient for the given solution. $\text{Re}_n(c_{m,a})$ and $\text{Im}_n(c_{m,a})$ are the real and imaginary components of the n -th Fourier mode of the moment coefficient for the accurate solution. According to the definitions in Eqs. (26) and (27), the results of error analysis for the lift and moment coefficients are shown in Fig. 10.

Figure 10a shows that for the flow with shock wave, the error in the lift coefficient using the BDF method decreases as the time resolution increases, and the drop rate of the error is less than 2. In the log-log coordinate system, if the temporal variation of the local pressure coefficient is smooth over the entire airfoil surface, then the drop rate of its error and the error of its integration quantities (such as lift coefficient) for the 2nd-order BDF method should be exactly 2. If a shock

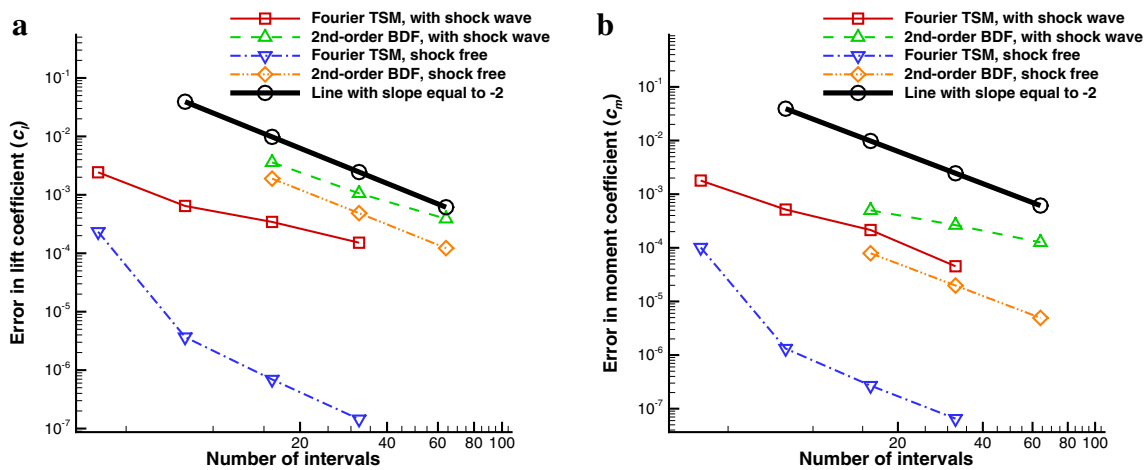


Fig. 10 Error of the computed solutions. **a** For lift coefficient. **b** For moment coefficient

wave occurs in some region of the airfoil surface, the temporal variation of the pressure coefficient is not smooth in the region. Thus, for the solutions of the 2nd-order BDF method, the drop rate of the error in the pressure coefficient and that of the lift coefficient all decrease below 2. Using the same time resolution, the error of the lift coefficient for the Fourier TSM is lower than that for the BDF method. This indicates that to obtain the lift coefficient with the same accuracy level, much fewer intervals are needed for the Fourier TSM. For instance, the lift coefficient calculated by the Fourier TSM with eight intervals is as accurate as the one obtained by the BDF method with 64 intervals. So it can be concluded that if the lift coefficient is taken as the figure-of-merit, the Fourier TSM is much more efficient than the 2nd-order BDF method even when shock wave occurs.

Figure 10a also shows that in the shock-free case, the drop rate of the error in the lift coefficient is exactly 2 for the 2nd-order BDF method. This is an expected result according to theoretical analysis. Under the same time resolution, the error in the lift coefficient for the Fourier TSM is much lower than that for the BDF method. For instance, the lift coefficient calculated by the Fourier TSM with only four intervals is as accurate as the one obtained by the BDF method with 64 intervals. This means if the lift coefficient is taken as the figure-of-merit, the Fourier TSM is extremely efficient for the shock-free case.

Figure 10b shows that the conclusion of the error analysis for the moment coefficient is similar to that for the lift coefficient. However, if the moment coefficient is taken as the figure-of-merit, the efficiency advantage of the Fourier TSM over the BDF method is weakened especially for the flow with shock wave. This is because the temporal variation of the moment coefficient is much more complicated than that of the lift coefficient if a shock wave occurs. For this reason, a higher time resolution is required for the Fourier TSM to

resolve the details of the temporal variation of the moment coefficient.

The above error analysis is made on the integral quantities of the surface pressure coefficient. In practice, the computational result of the surface pressure itself is also of great importance since it can reflect local flow details and key features. To evaluate the computational efficiency of the Fourier TSM more comprehensively, the error analysis should be conducted on the computed surface pressure coefficient as well. The following averaged squared error of the surface pressure coefficient can be defined for a given solution:

$$\begin{aligned}
 \text{Error}_{c_p, \text{averaged}}^2 = & \frac{1}{q} \sum_{s=1}^q \sum_{n=0}^m \left\{ [\text{Re}_n(c_p(s)) - \text{Re}_n(c_{p,a}(s))]^2 \right. \\
 & \left. + [\text{Im}_n(c_p(s)) - \text{Im}_n(c_{p,a}(s))]^2 \right\} \\
 & + \frac{1}{q} \sum_{s=1}^q \sum_{n=m+1}^{m_a} \left\{ [\text{Re}_n(c_{p,a}(s))]^2 \right. \\
 & \left. + [\text{Im}_n(c_{p,a}(s))]^2 \right\}, \tag{28}
 \end{aligned}$$

where $\text{Re}_n(c_p(s))$ and $\text{Im}_n(c_p(s))$ are the real and imaginary components of the n -th Fourier mode of the pressure coefficient for the given solution. $\text{Re}_n(c_{p,a}(s))$ and $\text{Im}_n(c_{p,a}(s))$ are the real and imaginary components of the n -th Fourier mode of the pressure coefficient for the accurate solution. q is the number of grid cells over the airfoil surface.

According to the definition in Eq. (28), the results of error analysis for the surface pressure coefficient is shown in Fig. 11. The average error of the surface pressure coefficient drops as time resolution increases in the similar trend that can be observed for the lift coefficient or the moment coefficient. However, for the flow with shock wave, the aver-

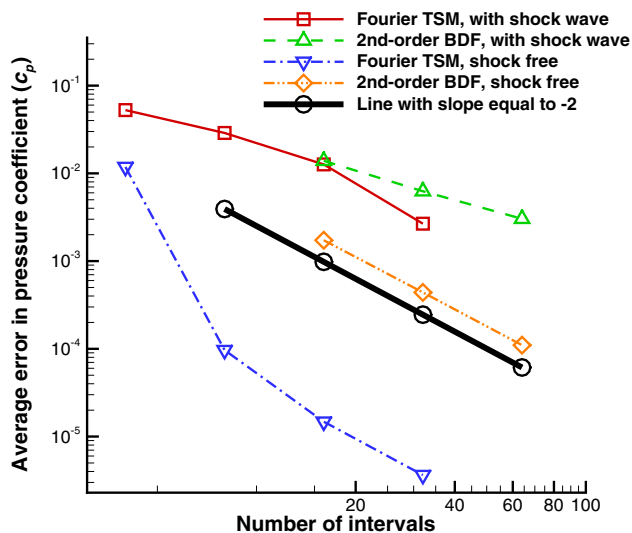


Fig. 11 Averaged error of the surface pressure coefficient

age error of the surface pressure coefficient for the Fourier TSM becomes comparable to that for the BDF method if the time resolution is relatively low (16 or fewer intervals are used in a period). For the flow with shock waves, the spectrum of the surface pressure coefficient contains significant components of higher modes due to the motion of the discontinuous shock wave. They only start to decay dramatically after the 7-th Fourier mode (seven modes are included if 16 intervals are used in a period). In the shock-free area, the spectrum of the surface pressure coefficient is much simpler and all Fourier modes decay rapidly. When time resolution is relatively low, the average error of the surface pressure coefficient mainly reflects the local error in the region of shock wave movement. In that region if 16 or fewer intervals are used, dominant Fourier modes are not included completely in the Fourier TSM. Hence, the aliasing error and the truncation error are high. Recall that the lift coefficient has a very simple spectrum and all of its Fourier modes decay rapidly. Hence, the temporal variation of lift coefficient can be predicted accurately by the Fourier TSM even when the time resolution is pretty low.

The above error analysis demonstrates that for integral quantities of the surface pressure coefficient (especially the lift coefficient) in flows with shock waves, the Fourier TSM is much more efficient than the BDF method. If the temporal variation of the surface pressure coefficient itself is simulated, the computational efficiency of the Fourier TSM decreases, but is still not lower than that of the BDF method. For the shock-free flow problems, the Fourier TSM is extremely efficient for both the surface pressure coefficient and its integral quantities.

Given the number of pseudo-time steps needed to reach convergence at each time instance being about the same, the total CPU time required by each method depends on the number of time instances to be computed in a period. The Fourier

TSM, being of exponential order of accuracy, achieves much higher time accuracy than the conventional 2nd-order BDF method, even for flows with shocks as discussed above. As a result, to achieve the same level of time accuracy, fewer time instances (intervals) in a period are needed for the Fourier TSM than for the conventional BDF time-marching method. For example, Fig. 11 shows that the Fourier TSM with eight time intervals achieves the same accuracy as the BDF with 64 time intervals for the shock-free case. In addition, to reach a steady-state periodic solution, the conventional time-marching solver has to go through an initial transient process by marching the real time forward for several (usually five or more) periods. With the Fourier TSM, however, the steady-state periodic solution is obtained in one shot by solving the coupled time-space equations without having to go through an extra transient period. Combining these two factors, the Fourier TSM is orders of magnitude faster than the conventional time-marching method for periodic flow problems where a high-order of accuracy in time is needed. In practice, however, the computational efficiency advantage of the Fourier TSM greatly hinges on the efficiency in solving the coupled system of Eq. (22) and also on the smoothness of the solutions. For problems where the solution contains discontinuities such as shock waves, the advantage of the Fourier TSM time may be reduced.

6 Application to the periodic problems with unknown frequency

In the preceding computations of the flows over the pitching NACA0012 airfoil, the frequency of the flow problems is known since it is equal to the given pitching frequency. For such computations, the Fourier TSM can be directly applied. Recall that the frequency is an explicit factor in the time spectral operator and it must be given for the Fourier TSM. There also exist flow problems in which the frequency is not known before experiments or computations. A representative flow problem of this kind is the laminar vortex shedding flow behind a circular cylinder. Though the flow is known to be periodic, the frequency is not known a priori. Only a rough estimation can be made by empirical formula. To obtain the accurate frequency and the unsteady flow field using the Fourier TSM or equivalent methods, a frequency searching process must be involved. McMullen et al. [17] proposed a gradient based variable time period (GBVTP) method for the frequency domain method. Gopinath and Jameson [18] proposed a similar gradient based method to the Fourier TSM. In the gradient-based method, the frequency is updated using the negative gradient of the squared unsteady residual with respect to frequency as follows

$$\omega^{l+1} = \omega^l - \alpha \frac{\partial \tilde{R}^2}{\partial \omega}, \quad (29)$$

where α is a coefficient that controls the update and it has to be carefully chosen to guarantee convergence. Given the initial guess of the frequency that is sufficiently close to the correct value, the method can find the exact frequency precisely.

To broaden the search range and make the initial guess of frequency less constrained, we propose a new method that is based on Fourier analysis of the lift coefficient (or another local or global flow variable) to estimate the frequency before the gradient-based method is used to obtain the final converged value. For problems like vortex shedding flow over a circular cylinder, the first Fourier mode of the lift coefficient usually achieves maximum amplitude. Applying Fourier analysis to the lift coefficient, the frequency of the Fourier mode with maximum amplitude can be assigned to be the new frequency. When the first mode of the lift coefficient reaches maximum amplitude, the gradient-based method takes over the duty of searching for the correct frequency.

In the present computation, a circular cylinder is fixed in the laminar flow at $M_\infty = 0.2$ and $Re = 180$. A 257×129 O-type mesh is used. The normal distance from the first grid point to the surface is 1×10^{-3} , while the cylinder diameter is unity. The far-field boundary of the mesh extends to about 200 diameters away from the cylinder. Based on the experience from the preceding computations, eight real-time intervals are employed when implementing the Fourier TSM. Since the present flow problem is shock-free, eight intervals should be sufficient to apply the Fourier TSM. Convergence criteria for the unsteady flow field is set to be 1×10^{-6} . The frequency search process doesn't stop until the flow field converges. The present computational result is compared with experimental data [24–27].

The convergence history is shown in Fig. 12a. Using the Fourier TSM and the proposed frequency search approach, the residual of the computation can finally drop to the conver-

Table 1 Vortex shedding flow behind circular cylinder

	St	Time-averaged c_d
Williamson [24,25]	0.1919	
Roshko [26]	0.185	
Henderson [27]		1.336
Current computation	0.1919	1.337

gence criteria. The frequency updating history with respect to multigrid cycles is shown in Fig. 12b. The non-dimensional angular frequency is defined as

$$\omega' = \frac{\omega d}{\sqrt{\frac{p_\infty}{\rho_\infty}}}, \quad (30)$$

where d is diameter of cylinder, p_∞ the free-stream pressure, and ρ_∞ the free-stream density. The initial non-dimensional angular frequency is about 0.0237 (the corresponding reduced frequency is 0.05), while the final converged non-dimensional angular frequency is 0.2852. The initial guess of the frequency is far away from the correct value.

Finally, the Strouhal number is found and the converged time-averaged drag coefficient of the present computation are compared with experimental data in Table 1. For the Strouhal number, the current computational result is very close to Williamson's [24,25] data. For the time-averaged drag coefficient, the current computational result matches Henderson's [27] data very well.

In the present computation, Fourier analysis of the lift coefficient is carried out after every 100 multigrid cycles. The histories of lift coefficient at different time levels with respect to multigrid cycles are shown in Figs. 13, 14, and 15. Figure 13a shows that during the first 100 multigrid cycles,

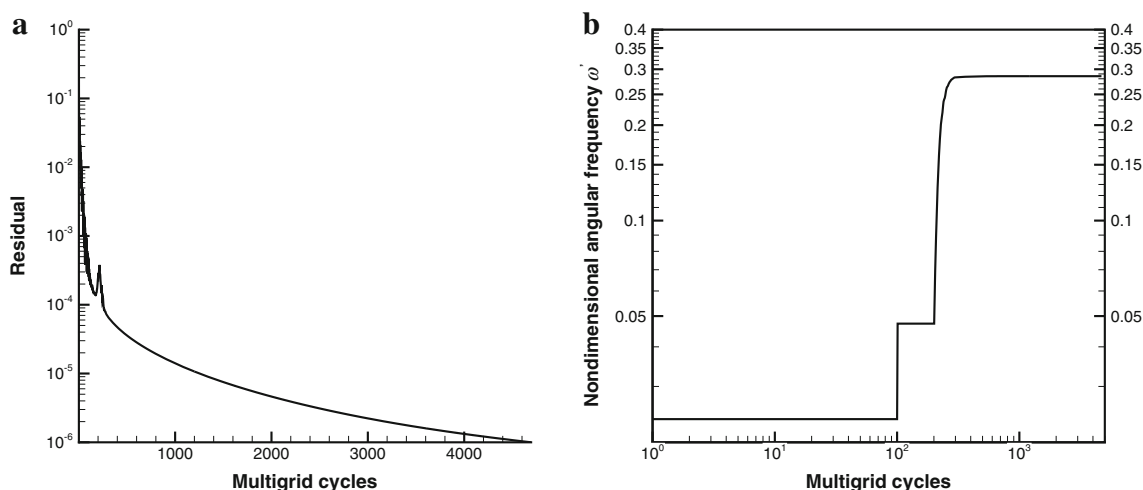


Fig. 12 Convergence history of the flow over circular cylinder case. **a** History of residual. **b** History of computed frequency ω'

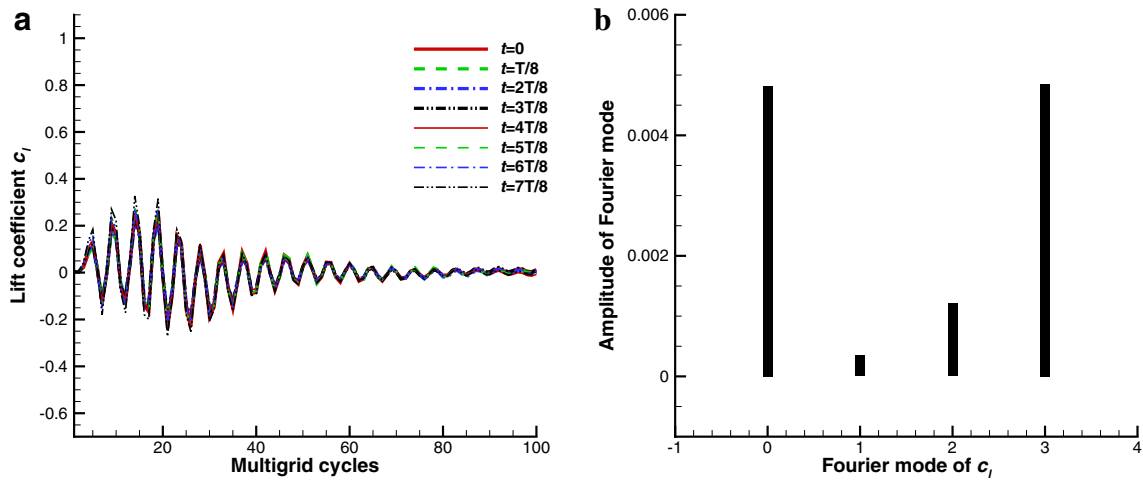


Fig. 13 Flow over circular cylinder: lift coefficient and its Fourier spectrum in multigrid cycle 1–100. **a** c_l history in multigrid cycle 1–100. **b** Spectrum of c_l at the end of multigrid cycle 100

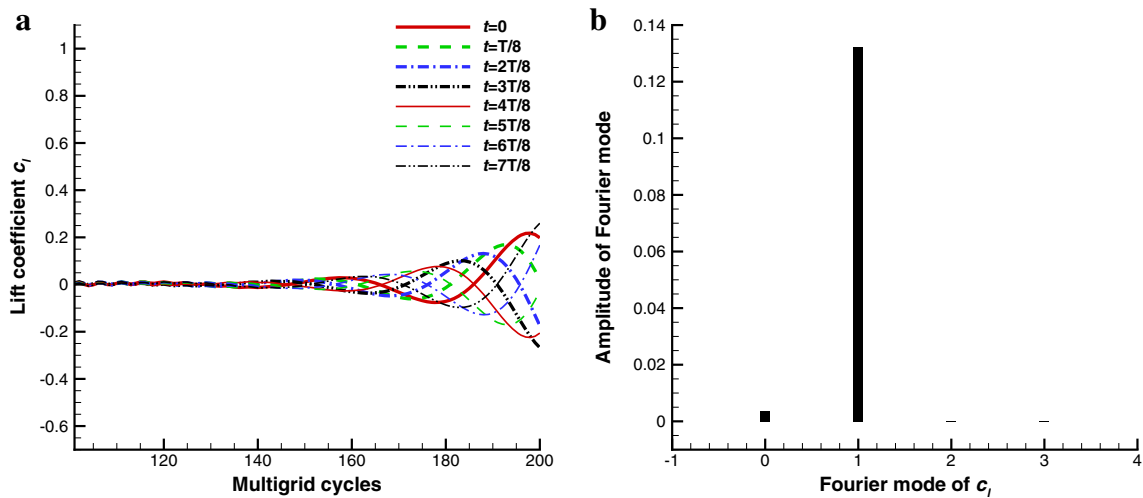


Fig. 14 Flow over circular cylinder: lift coefficient and its Fourier spectrum in multigrid cycle 101–200. **a** c_l history in multigrid cycle 101–200. **b** Spectrum of c_l at the end of multigrid cycle 200

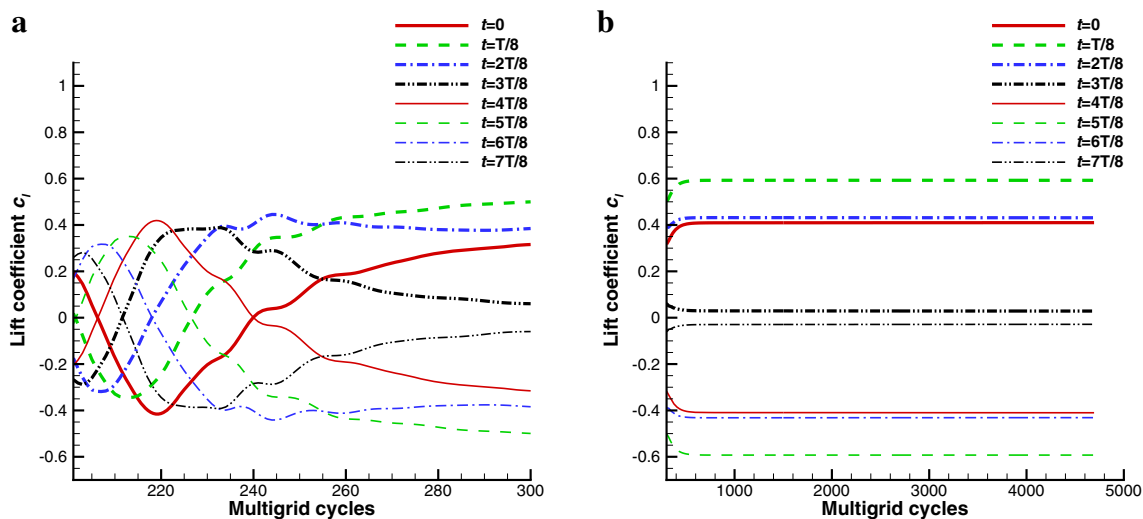


Fig. 15 Flow over circular cylinder: lift coefficient in multigrid cycles after 200. **a** c_l history in multigrid cycle 201–300. **b** c_l history after multigrid cycle 300

the lift coefficient at different time levels generally oscillate with the same phase. However, a phase difference starts to appear near the 100-th multigrid cycle. Figure 13b shows that at the end of the 100-th multigrid cycle, the third Fourier mode of the lift coefficient achieves maximum amplitude. Since the third Fourier mode is the one with the highest frequency that the Fourier TSM with eight intervals can include, the overall error of this mode is usually the highest among the included Fourier modes. For this reason, the frequency of the second Fourier mode is assigned as the new frequency. Figure 14a shows that in the next 100 multigrid cycles, the lift coefficient on different time levels continues to oscillate with phase difference. However, the amplitude of the oscillation is growing gradually. Figure 14b shows that at the end of the 200-th multigrid cycle, the first Fourier mode of the lift coefficient already achieves maximum amplitude. So

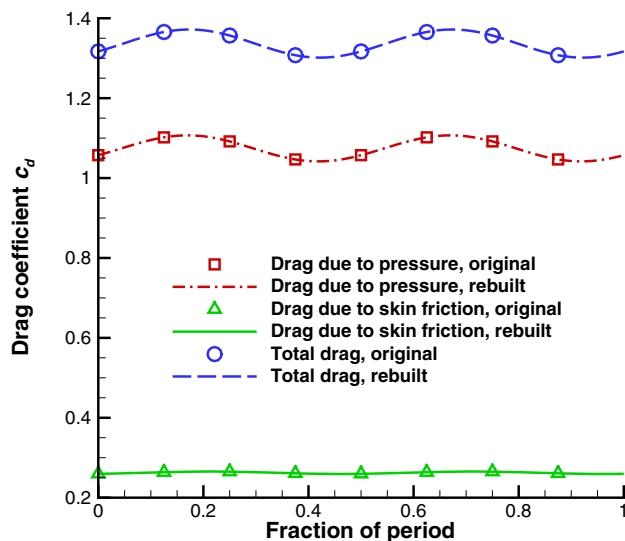


Fig. 16 Flow over circular cylinder: drag coefficients in a period

from the 201-th multigrid cycle, the gradient based method starts to search the correct frequency. In the third 100 multigrid cycles, Fig. 15a shows that the lift coefficient on each time level stops oscillating gradually and approaches its converged value. After that, the lift coefficient on each time level completely stops oscillating and finally converged. This is illustrated in Fig. 15b.

The temporal variations of the total drag coefficient and its components due to pressure and skin friction in a period are shown in Fig. 16. The original discrete computational results, as well as the rebuilt results are plotted. The rebuilt results are obtained by summing the resolved Fourier modes on 129 equally spaced instants over the obtained period. It can be observed that the drag due to pressure is the dominant component of the total drag. The mean value and the variation amplitude of the drag due to pressure are all much larger than those of the drag due to skin friction. The temporal variations of the lift and moment coefficients in a period are shown in Fig. 17.

Figure 18 shows the vortex shedding process during one shedding period. Mach number contours in flood type and streamlines are plotted using the present computational results. Every vortex in this flow is initially generated on the surface area near the trailing edge, then it grows larger progressively. When the vortex is about the size of the cylinder, it detaches from the surface. After that, the detached vortex sheds away from the cylinder and dissipates in the wake. This process occurs alternately on upper and lower surface area near the trailing edge.

7 Conclusion

The Fourier TSM for the unsteady Navier–Stokes equations is presented and tested for a transonic flow over a pitching

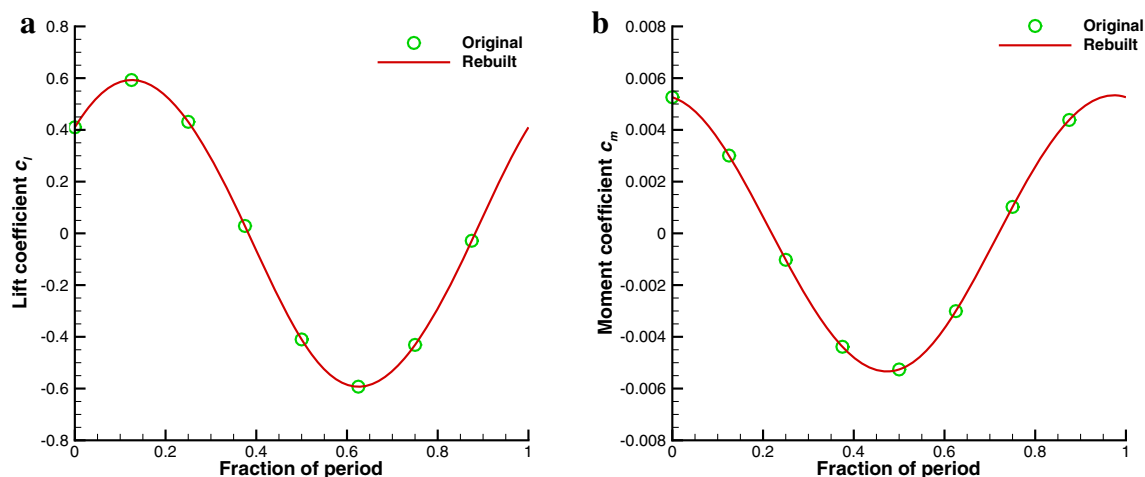


Fig. 17 Flow over circular cylinder: lift and moment coefficients in a period. **a** Lift coefficient. **b** Moment coefficient

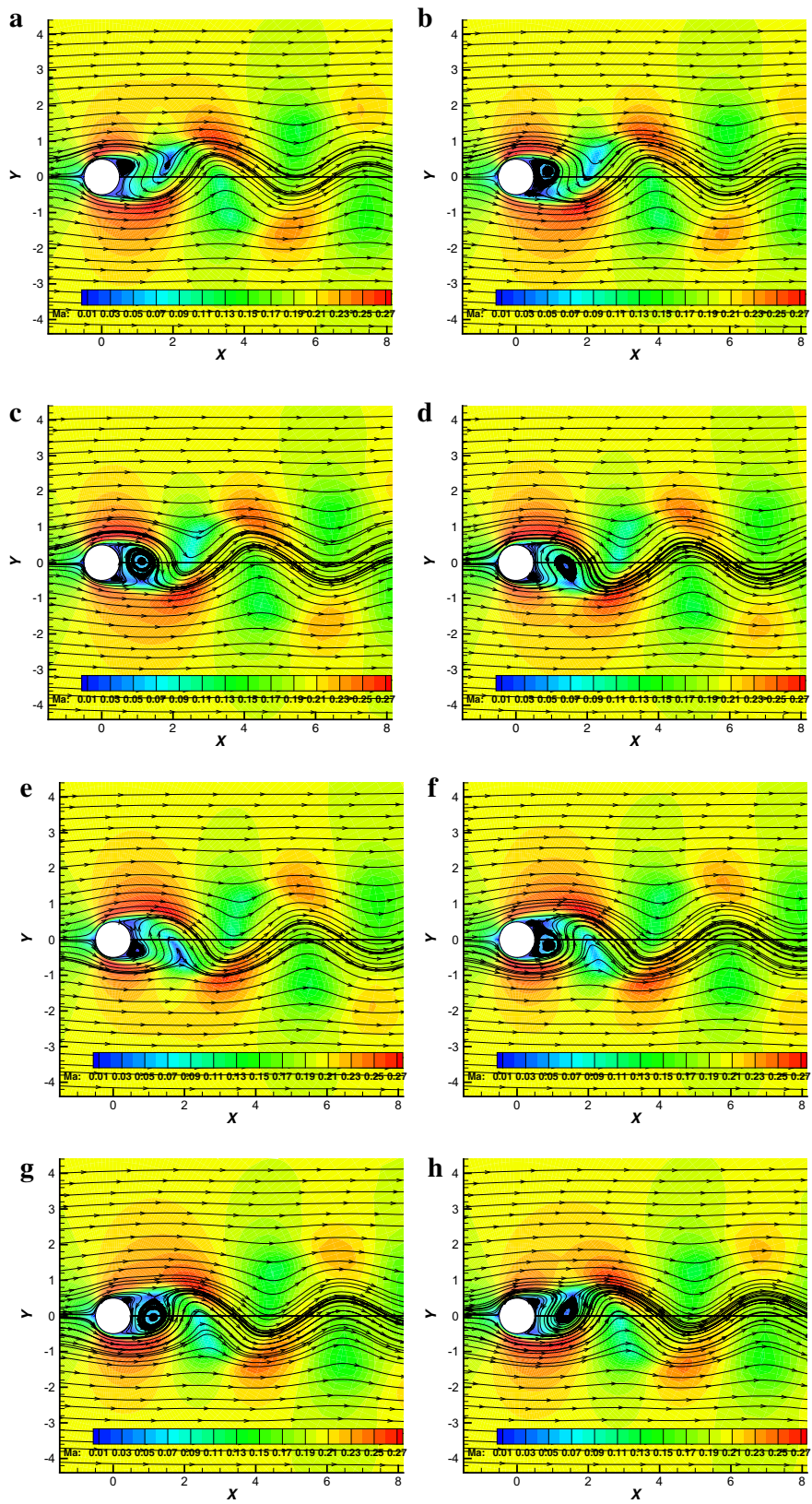


Fig. 18 Flow over circular cylinder: mach number contours and stream lines during one vortex shedding period. **a** $t = 0$. **b** $t = \frac{1}{8}T$. **c** $t = \frac{2}{8}T$. **d** $t = \frac{3}{8}T$. **e** $t = \frac{4}{8}T$. **f** $t = \frac{5}{8}T$. **g** $t = \frac{6}{8}T$. **h** $t = \frac{7}{8}T$

NACA0012 airfoil and compared with the results of using a conventional 2nd-order BDF method. Convergence study of the time discretization errors with respect to the number of time steps for the two methods show that the Fourier TSM offers significantly better accuracy than the second-order BDF method for predicting both the local pressure coefficient and integrated force coefficients for subsonic periodic flows. For transonic periodic flows where the motion of the discontinuous shock wave contributes significant higher-order harmonic components to the local pressure, a sufficient number of modes must be included before the Fourier TSM provides an advantage over the BDF method. For example, more than 16 time intervals are needed in a period for the Fourier TSM to resolve the surface pressure coefficient in regions of the shock-wave movement for the oscillating airfoil problem. The Fourier TSM, however, still offers better accuracy than the BDF method for integrated force coefficients even for flows with shock waves. Computations also reveal a problem of non-symmetric solutions occurring for symmetric periodic flows due to the use of odd numbers of intervals. This non-symmetry is accentuated for the Fourier TSM for transonic flows when an insufficient number of harmonic modes are included.

For problems where the frequency is not known a priori, a search algorithm based on a combination of Fourier analysis of the computed time-history of a flow quantity and a gradient method based on minimizing the unsteady residual of the Navier–Stokes equations can be used to quickly and accurately determine the frequency of the flow. This frequency-search method along with the Fourier TSM are successfully demonstrated for the periodic vortex shedding problem of the low Reynolds number flow over a circular cylinder. Fourier analysis of the lift coefficient is first performed to estimate the unknown frequency before the gradient method is used to pin down the final value. The method works for initial guesses of the frequency that are far away from the correct value. The Fourier TSM gives excellent prediction of the drag value and the Strouhal number compared to experimental data with as few as only eight time intervals for this vortex shedding flow problem.

Acknowledgments The research was supported by the State Scholarship Fund of the China Scholarship Council (Grant 2009629129).

References

1. Yao, J., Jameson, A., Alonso, J.J., et al.: Development and validation of a massively parallel flow solver for turbomachinery flows. *J. Propuls. Power* **17**, 659–668 (2001)
2. Sadeghi, M., Liu, F.: Investigation of mistuning effects on cascade flutter using a coupled method. *J. Propuls. Power* **23**, 266–272 (2007)
3. Liu, F., Cai, J., Zhu, Y., et al.: Calculation of wing flutter by a coupled fluid-structure method. *J. Aircr.* **38**, 334–342 (2001)
4. Xiao, Q., Tsai, H.M., Liu, F.: Numerical study of transonic buffet on a supercritical airfoil. *AIAA J.* **44**, 620–628 (2006)
5. Xiong, J., Nielsen, P., Liu, F., et al.: Computation of high-speed coaxial jets with fan flow deflection. *AIAA J.* **48**, 2249–2262 (2010). doi:10.2514/1.51645
6. He, G.W., Rubinstein, R., Wang, L.P.: Effects of subgrid-scale modeling on time correlations in large eddy simulation. *Phys. Fluids* **14**, 2186–2193 (2002)
7. He, G.W., Wang, M., Lele, S.K.: On the computation of space-time correlations by large-eddy simulation. *Phys. Fluids* **16**, 3859–3867 (2004)
8. Yang, Y., He, G.W., Wang, L.P.: Effects of subgrid-scale modeling on lagrangian statistics in large eddy simulation. *J. Turbul.* **9**, 1–24 (2008)
9. Jin, G.D., He, G.W., Wang, L.P.: Large-eddy simulation of turbulent-collision of heavy particles in isotropic turbulence. *Phys. Fluids* **22**, 1–13 (2010)
10. Jameson, A.: Time dependent calculations using multigrid, with applications to unsteady flows past airfoils and wings. In: *AIAA 10th Computational Fluid Dynamics Conference*, AIAA-91-1596 (1991)
11. Liu, F., Ji, S.: Unsteady flow calculations with a multigrid Navier–Stokes method. *AIAA J.* **34**, 2047–2053 (1996)
12. Hall, K.C., Crawley, E.F.: Calculation of unsteady flows in turbomachinery using the linearized Euler equations. *AIAA J.* **27**, 777–787 (1989)
13. Ning, W., He, L.: Computation of unsteady flows around oscillating blades using linear and nonlinear harmonic Euler methods. *ASME J. Turbomach.* **120**, 508–514 (1998)
14. Hall, K.C., Thomas, J.P., Clark, W.S.: Computation of unsteady nonlinear flows in cascades using a harmonic balance technique. *AIAA J.* **40**, 879–886 (2002)
15. Gopinath, A.K., Weide, E., Alonso, J.J., et al.: Three-dimensional unsteady multi-stage turbomachinery simulations using the harmonic balance technique. In: *45th AIAA Aerospace Sciences Meeting & Exhibit*, AIAA-2007-0892 (2007)
16. Ekici, K., Hall, K.C., Dowell, E.H.: Computationally fast harmonic balance methods for unsteady aerodynamic predictions of helicopter rotors. In: *46th AIAA Aerospace Sciences Meeting & Exhibit*, AIAA-2008-1439 (2008)
17. McMullen, M., Jameson, A., Alonso, J.J.: Application of a nonlinear frequency domain solver to the Euler and Navier–Stokes equations. In: *40th AIAA Aerospace Sciences Meeting and Exhibit*, AIAA-2002-0120 (2002)
18. Gopinath, A.K., Jameson, A.: Application of the time spectral method to periodic unsteady vortex shedding. In: *44th AIAA Aerospace Sciences Meeting & Exhibit*, AIAA-2006-0449 (2006)
19. McMullen, M., Jameson, A.: The computational efficiency of nonlinear frequency domain methods. *J. Comput. Phys.* **212**, 637–661 (2006)
20. Jameson, A., Schmidt, W., Turkel, E.: Numerical solution of the Euler equations by finite volume methods using Runge–Kutta time stepping schemes. In: *AIAA 14th Fluid and Plasma Dynamic Conference*, AIAA-81-1259 (1981)
21. Landon, R.H.: NACA0012 oscillation and transient pitching, compendium of unsteady aerodynamic measurements, data set 3. AGARD Technical Report No.702 (1982)
22. Gao, C., Yang, S., Luo, S., et al.: Calculation of airfoil flutter by and Euler method with approximate boundary condition. *AIAA J.* **43**, 295–305 (2005)
23. Gao, C., Luo, S., Liu, F.: Numerical solution of the unsteady Euler equations for airfoils using approximate boundary conditions. *Acta Mech. Sin.* **19**, 427–436 (2003)
24. Williamson, C.H.K.: Defining a universal and contiguous Strouhal–Reynolds number relationship of the laminar vortex shedding of a

- circular cylinder. *Phys. Fluids* **31**, 2742–2744 (1988). doi:[10.1063/1.866978](https://doi.org/10.1063/1.866978)
25. Williamson, C.H.K.: Measurements of base pressure in the wake of a cylinder at low Reynolds numbers. Technical report 14, *Z. Flugwiss, Weltraumforsch*, 38–46 (1990)
26. Roshko, A.: On the development of turbulent wakes from vortex streets. NACA Technical Note No.1191 (1953)
27. Henderson, R.D.: Details of the drag curve near the onset of vortex shedding. *Phys. Fluids* **7**, 2102–2104 (1995). doi:[10.1063/1.868459](https://doi.org/10.1063/1.868459)